European Journal of Pharmaceutics and Biopharmaceutics 137 (2019) 148–163

Contents lists available at ScienceDirect

European Journal of Pharmaceutics and Biopharmaceutics

journal homepage: www.elsevier.com/locate/ejpb

Research paper

Effect of preparation method on the surface properties and UV imaging of indomethacin solid dispersions

Kofi Asare-Addo[a,*], Maen Alshafiee[a], Karl Walton[b], Adam Ward[a], Ana-Maria Totea[a], Sadaf Taheri[a], Nihad Mawla[a], Adeola O. Adebisi[a], Sheima Elawad[a], Chantel Diza[a], Peter Timmins[a], Barbara R. Conway[a]

[a] Department of Pharmacy, University of Huddersfield, Huddersfield HD1 3DH, UK
[b] EPSRC Future Metrology Hub, University of Huddersfield, Huddersfield HD1 3DH, UK

ARTICLE INFO

Keywords:
Indomethacin
Soluplus
Amorphous solid dispersions
UV imaging
Surface dissolution imaging
Focus variation

ABSTRACT

This work explores the use of UV imaging in solid dispersion systems. Solid dispersions are one of the common strategies used in improving the dissolution of poorly soluble drugs. Three manufacturing techniques (spray drying (SD), freeze drying (FD) and homogenising (HG)) are investigated. Differential Scanning Calorimetry (DSC) and X-Ray Powder Diffraction (XRPD) was used in characterising the solid dispersions. Advanced imaging was implemented to give an insight into how these solid dispersions performed. The DSC and XRPD results showed that all three methods and the various ratios studied produced amorphous solid dispersions. Ultra-Violet (UV) imaging of the pseudo Intrinsic Dissolution Rate (IDR) deduced only two samples to have superior pseudo IDR values to the IDR of the parent drug indomethacin (INDO). The whole dose imaging of the capsule formulation however showed all the samples (SD, FD and HG) to have superior dissolution to that of INDO which was in contrast to the IDR results. The UV images obtained from the determination of the pseudo IDR also showed a phenomenon the authors are reporting for the first time where increased polymer (Soluplus) content produced "web-like" strands that migrated to the top of the quartz cell which may have been responsible for the low pseudo IDR values. The authors also report for the first time using this UV imaging technique, the tip of a capsule coming off for drug to go into solution. The area under the curve suggested the best five samples dissolution wise to be 1:3 SD > 1:1 HG > 1:1 SD > 1:3 FD > 1:3 HG meaning a ratio of INDO to SOL in these dispersion of up to 1:3 being sufficient to produce significant dissolution increases. The developed interfacial (surface) area ratio (Sdr) highlighted how the surface area of the IDR compacts varied between the batches, in particular highlighting larger surface area gains for the FD and HG compacts. A choice of instrumentation/techniques to use in making solid dispersions may well come down to cost or instrument availability for a formulator as all three techniques were successful in improving the dissolution of indomethacin. This work thus highlights the importance of having both complimentary IDR and whole dosage imaging techniques in giving a better understanding of solid dispersion systems.

1. Introduction

It is currently estimated that over 80% of new chemical entities (NCE) have poor aqueous solubility [1]. The challenge faced by the pharmaceutical industry is thus improving the solubility of poorly water-soluble drugs to enhance their performance *in-vivo*, and ultimately to maximise bioavailability. The Biopharmaceutical Classification System (BCS) classifies most of these active pharmaceutical ingredients (API) as belonging to Class II [2,3]. BCS Class II drugs have low solubility and high membrane permeability, and ultimately dissolution is the rate-limiting step for the drug to be released from its dosage formulation [4]. The improvement of solubility in poorly soluble drugs can be challenging, costly and time-consuming. As such, choosing the correct technique is essential and to date, there are several

Abbreviations: NCE, new chemical entities; API, active pharmaceutical ingredients; BCS, biopharmaceutical classification system; INDO, indomethacin; SOL, soluplus; PEG, polyethene glycol; PVP, polyvinylpyrrolidone; HPMC, hydroxypropyl methylcellulose; SDI, surface dissolution imaging; IDR, intrinsic dissolution rate; DSC, differential scanning calorimetry; XRPD, X-ray powder diffraction; SEM, scanning electron microscopy; SD, spray dried; FD, freeze dried; HG, homogenised

* Corresponding author.
E-mail address: k.asare-addo@hud.ac.uk (K. Asare-Addo).

https://doi.org/10.1016/j.ejpb.2019.03.002
Received 9 November 2018; Received in revised form 21 January 2019; Accepted 1 March 2019
Available online 02 March 2019
0939-6411/

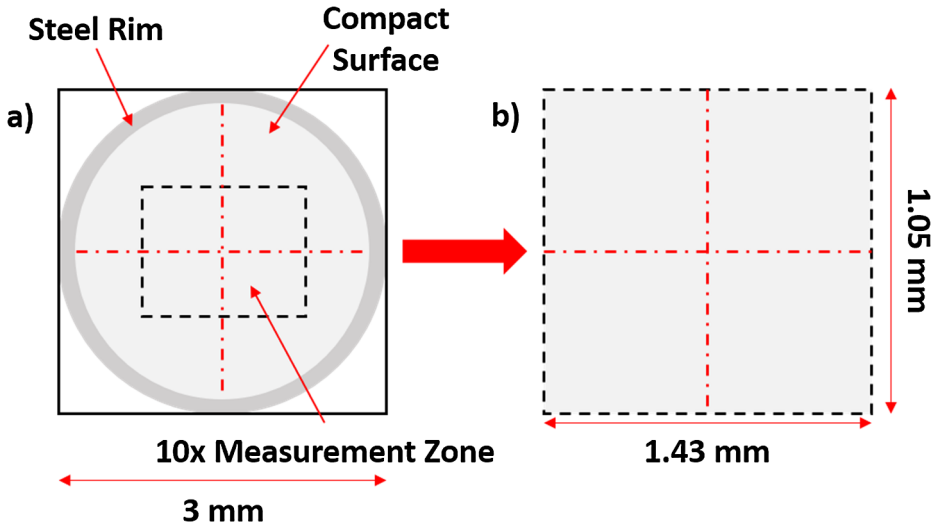

Fig. 1. (a) Schematic representation of the measurement zone for the 10× magnification used (b) 10× magnification field from which the developed interfacial (surface) area ratio (Sdr) and texture aspect ratio (Str) was determined.

methods including salt formation, liquisolid techniques, complexation, cocrystals, particle size reduction, solid dispersion and the use of additives in the crystallisation process in overcoming this challenge [5–24]. Solid dispersion is a widely used method and has resulted in successful improvements of solubility and bioavailability of poorly soluble APIs. The challenge often is the selection of an appropriate carrier [25] with most often opting for synthetic or naturally water-soluble polymers such as polyethene glycol (PEG), soluplus, polyvinylpyrrolidone (PVP) or hydroxypropyl methylcellulose (HPMC) for a successful formulation in which the API is often molecularly dispersed within the carrier [21,26–30].

Intrinsic dissolution rate (IDR) is an important parameter that can help to predict API behaviour *in vivo* and is determined in the early stages in drug development. Intrinsic dissolution rates above 0.1 mg min^{-1} cm^{-2} of APIs are generally considered highly soluble whereas rates below this limit often indicate the API has low solubility [31]. One of the aims in this research paper is to explore the effect of three preparation methods on IDR values of a model drug indomethacin (INDO) and its pseudo IDR for its solid dispersions with Soluplus. The Surface Dissolution Imaging (SDI) instrument (Pion Inc, USA), has been used for various applications as well as determining IDRs for APIs due to its compound sparing approach [16,32–41]. SDI has also been used to evaluate solid dispersions of nilotinib with hydroxypropyl methylcellulose phthalate [42]. This instrument typically requires 5–10 mg of an API with an experimental run time of about 20–30 min in IDR determinations. The SDI also supports a wide range of wavelengths allowing a diverse range of analysis albeit only one wavelength can be used at a time. The version 2 of the of the SDI instrument (SDI2), now has the ability to record UV data at 2 wavelengths simultaneously with a range of wavelengths (255, 280, 300 and 320 nm) in determining IDR values. This work also uses a focus variation instrument (Alicona Imaging GmbH, Graz, Austria) to provide information with regards to the surface metrology of the compacts prepared pre IDR or pseudo IDR measurements to give insights as to the influence of the manufacturing process on the topography of compacts. This technology used in micro-precision manufacturing is typically used for quality assurance [43–45] and acquires topographic surface height data in profile (2D) and areal (3D) formats along with true colour surface images. The SDI2 also has an additional wavelength of 520 nm that allows the imaging of events at a visible wavelength to be recorded [46]. The authors have also aimed at exploiting the dual wavelength capability of this instrument as well as its ability to image a whole dosage form (capsule in this case) in providing insights on the drug release and capsule dissolution process which we believe we are reporting for the first time. These advanced imaging techniques are of great importance to a formulator due to the added knowledge it provides in better understanding these formulations

2. Materials and methods

2.1. Materials

Indomethacin was purchased from TCI Chemicals, UK. Soluplus was a kind gift from BASF, Germany. The solvents methanol and ethanol used in the preparation of the solid dispersions were of analytical grade and were purchased from Fisher (UK). Phosphate buffer (pH 7.2) was the media used for IDR or pseudo IDR determination, solubility testing as well as whole dosage imaging and was prepared according to the USP 2003 using sodium hydroxide and potassium phosphate monobasic purchased from Fisher (UK) and Acros Organics (Germany) respectively.

2.2. Methods for solid dispersion preparations

2.2.1. Preparation of spray dried INDO:SOL solid dispersions

Appropriate amounts of INDO (8 g at all ratios used) and SOL making the ratios 1:1, 1:3 and 1:5 by weight were made by dissolving INDO and SOL in ethanol (1.6 L) under stirring condition (200 rpm). The resultant solutions made were then spray dried using the Labplant Spray Drier under the following conditions: pump setting 15 (equivalent to 695 mL/h), fan setting at 25 (equivalent to 3.25 m/s) and an inlet temperature of 90 °C. The collected spray dried particles from the three ratios studied were stored in a desiccator at room temperature until required.

2.2.2. Preparation of freeze dried INDO:SOL solid dispersions

1 g INDO was weighted and dissolved in 100 mL of methanol under stirring conditions on a hot plate (200 rpm at 70 °C to aid IND dissolution). In another beaker, 1 g SOL was also dissolved under stirring conditions at room temperature in 100 mL deionised water. The beaker

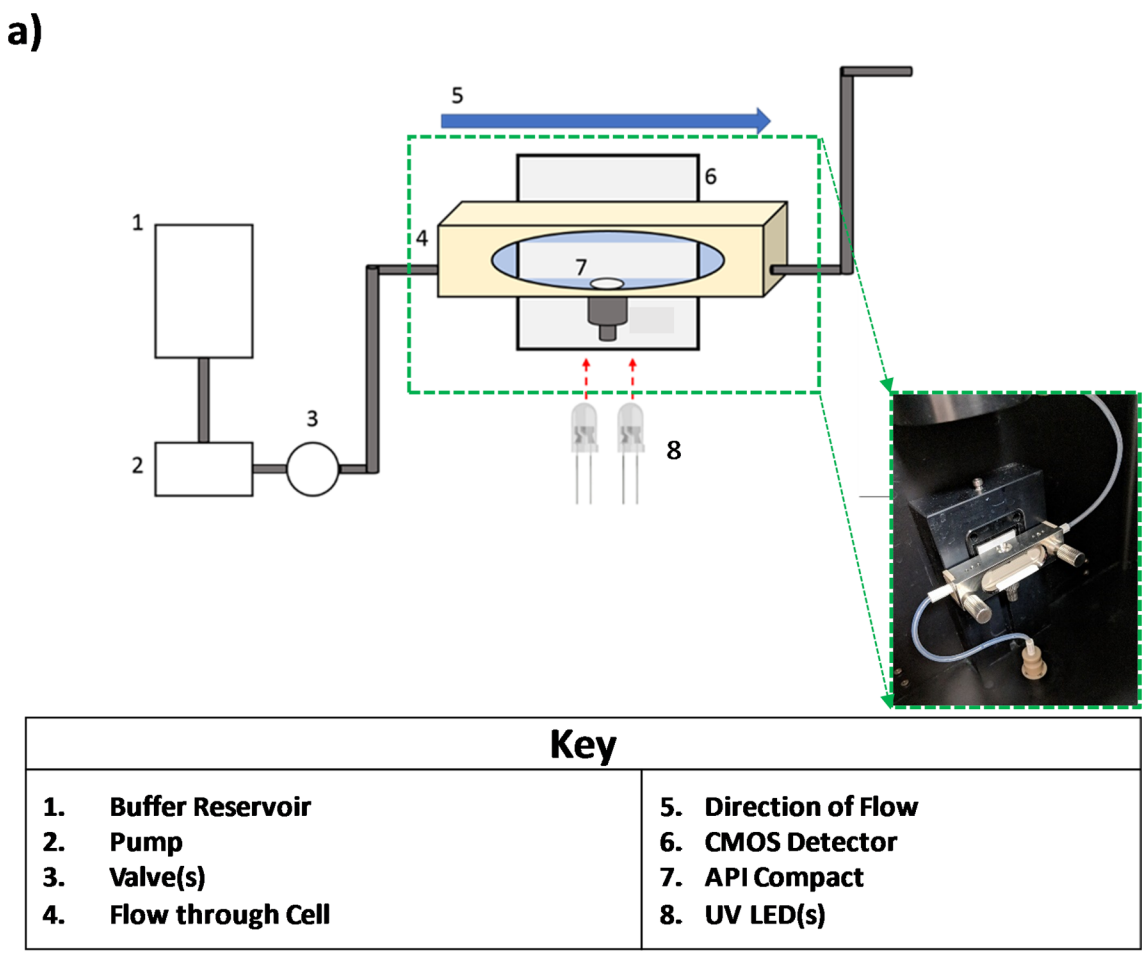

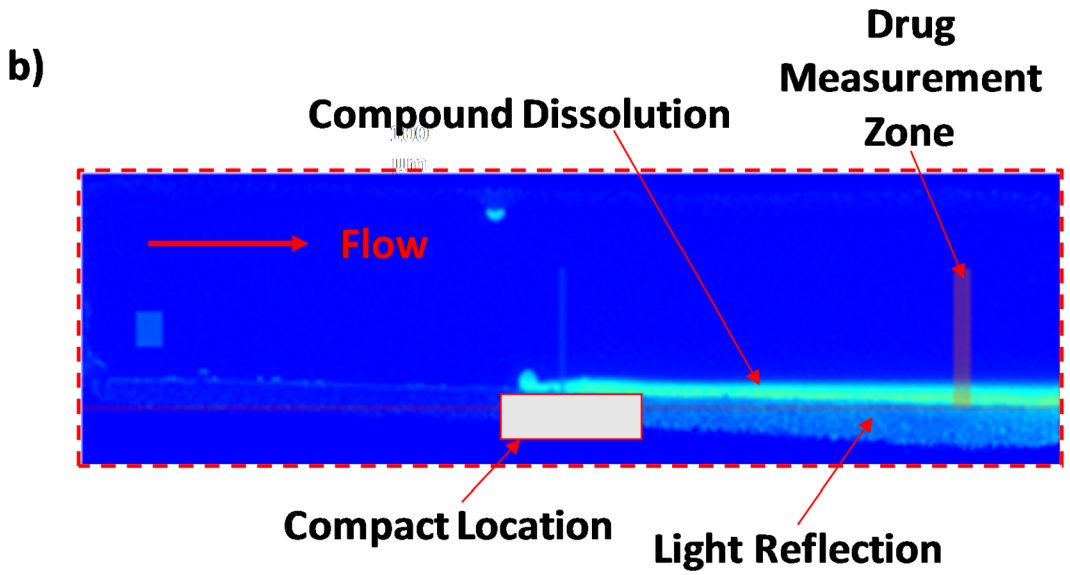

Fig. 2. (a) A schematic representation of the flow through set-up for the SDI2 UV imaging system (b) A typical image produced from an intrinsic dissolution rate experiment with the various aspects of analysis.

containing INDO was gradually introduced to the beaker containing SOL under stirring (500 rpm at 70 °C to aid solvent evaporation prior to freeze drying). The resultant sample was then immersed in liquid nitrogen to freeze prior to freeze drying using the Christ Alpha 2–4 LD Plus freeze drier. This sample was collected after it had been freeze dried and labelled 1:1, stored until required. The same process was

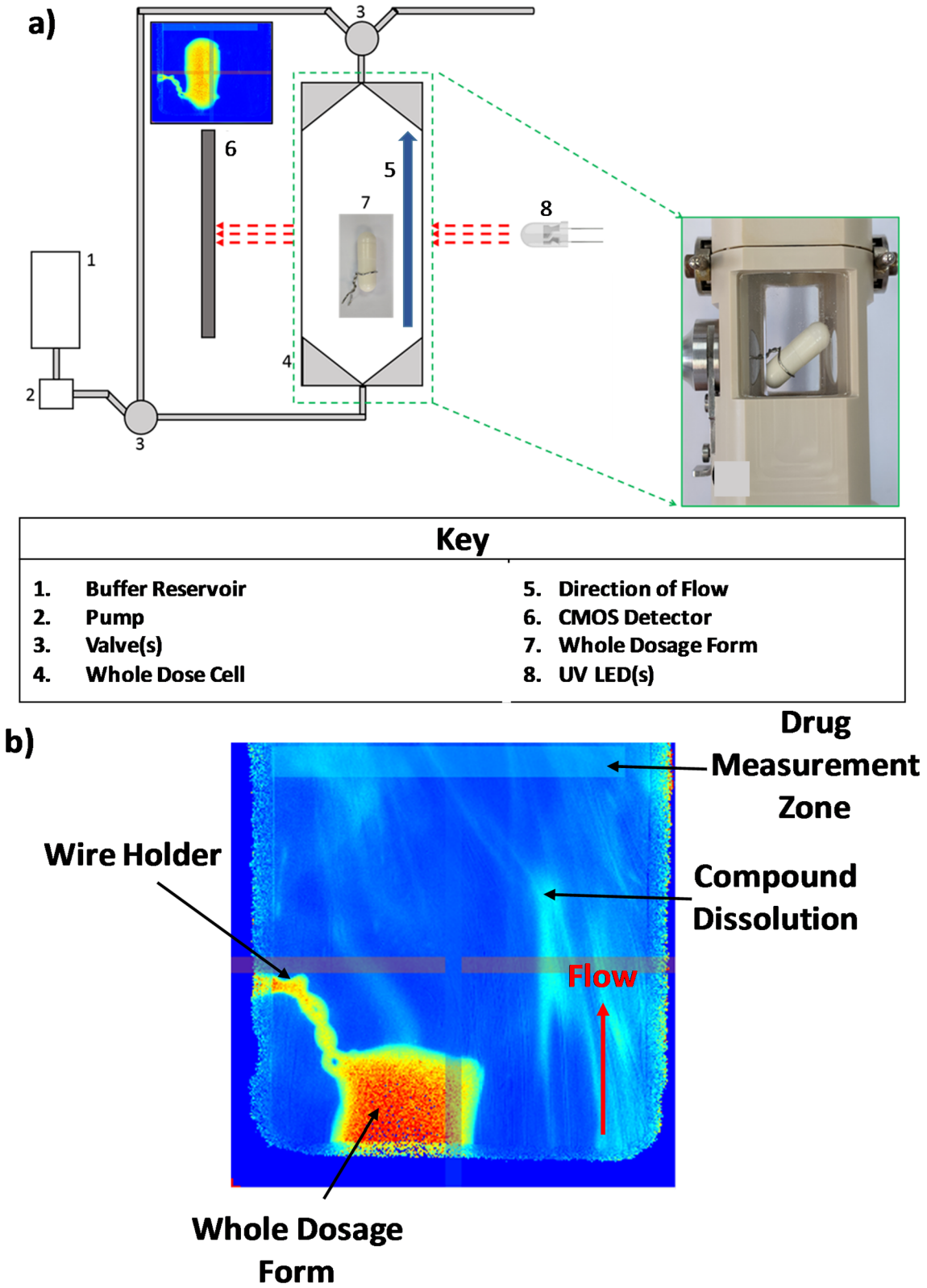

Fig. 3. (a) A schematic representation of the whole dose set-up for the SDI2 UV imaging system (b) A typical image produced from a whole dosage assessment with the various aspects of analysis.

employed with regards to making the 1:3 and 1:5 IND:SOL solid dispersions with the only difference being 3 g or 5 g being used for SOL respectively to account for its ratio.

2.2.3. Preparation of homogenised INDO:SOL solid dispersions

A similar methodology as reported in Section 2.2.2 was adopted and modified. Three beakers containing 1 g, 3 g or 5 g SOL in 100 mL

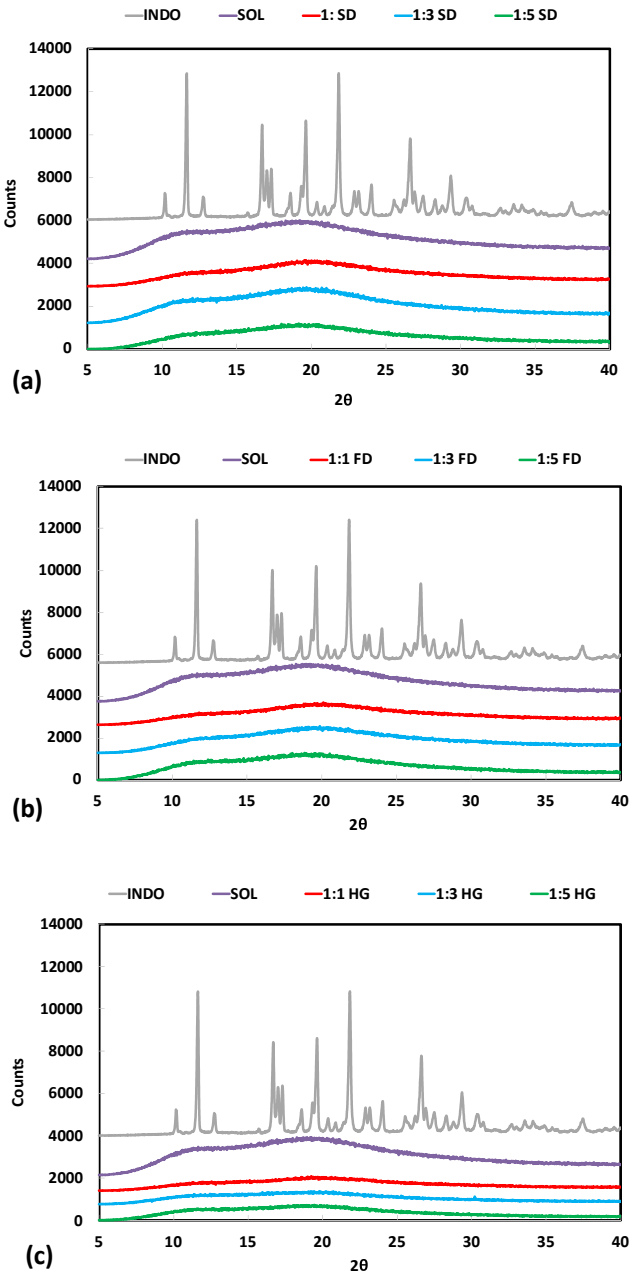

Fig. 4. XRPD analysis for the (a) INDO drug, SOL and the 1:1 SD, 1:3 SD and 1:5 SD dispersions, (b) INDO drug, SOL and the 1:1 FD, 1:3 FD and 1:5 FD dispersions, (c) INDO drug, SOL and the 1:1 HG, 1:3 HG and 1:5 HG dispersions.

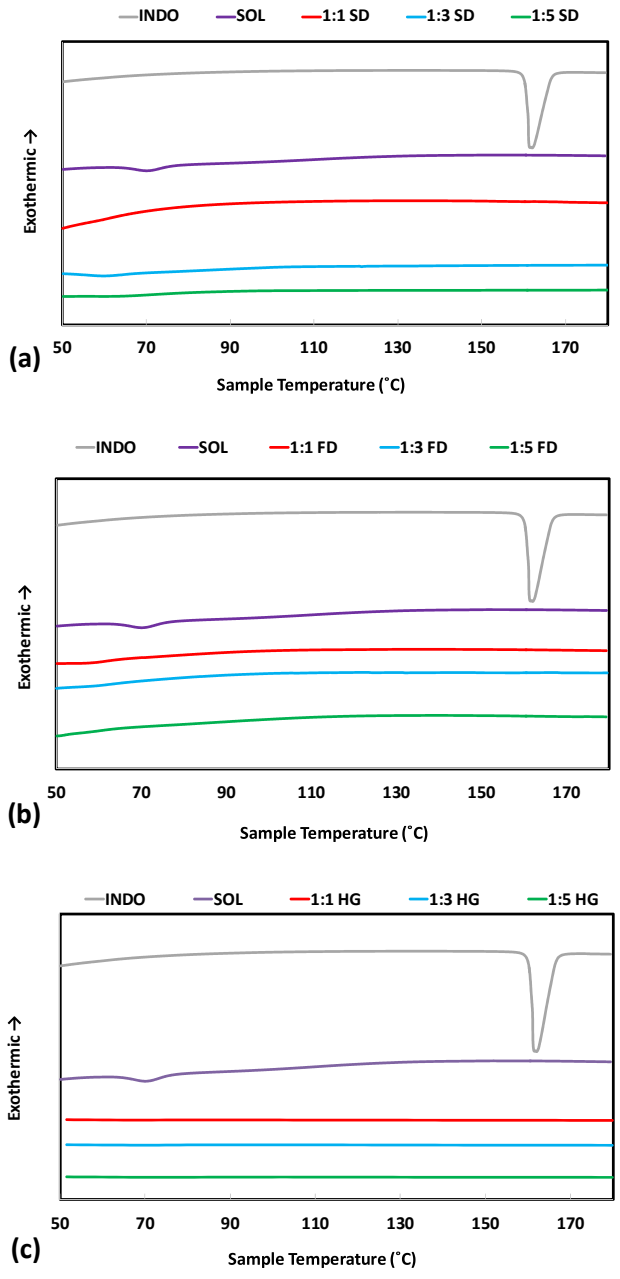

Fig. 5. DSC traces for the (a) INDO drug, SOL and the 1:1 SD, 1:3 SD and 1:5 SD dispersions, (b) INDO drug, SOL and the 1:1 FD, 1:3 FD and 1:5 FD dispersions, (c) INDO drug, SOL and the 1:1 HG, 1:3 HG and 1:5 HG dispersions.

deionised water under stirring conditions were prepared. Another beaker containing a concentrated amount of dissolved INDO in methanol equal to 1 g IND in a 20 mL syringe was prepared. Firstly, the beaker containing the 1 g SOL in 100 mL was placed under a high pressure homogeniser. A syringe containing 20 mL of the concentrated IND (equivalent to 1 g INDO) was added dropwise to the beaker containing 1 g SOL (1000 rpm for 10 min). The obtained suspension was then immersed in liquid nitrogen to freeze prior to freeze drying using the Christ Alpha 2–4 LD Plus freeze drier. This same process was repeated to give the 1:3 and 1:5 ratios. The collected homogenised and freeze dried particles from the three ratios were then stored in a desiccator until required. This method was used to determine if homogenising had an effect on the freeze-dried samples.

2.3. Solid state characterisation

2.3.1. Scanning electron microscopy (SEM)

Prior to observation on a scanning electron microscope (Jeol JSM-6060CV SEM), each sample (INDO, SOL, SD1:1 (1:1 ratio-spray dried sample), SD1:3 (1:3 ratio-spray dried sample), SD1:5 (1:5 ratio-spray dried sample), FD1:1 (1:1 ratio-freeze dried sample), FD1:3 (1:3 ratio-freeze dried sample), FD1:5 (1:5 ratio-freeze dried sample), HG1:1 (1:1 ratio-homogenised dried sample), HG1:3 (1:3 ratio- homogenised dried sample) and HG1:5 (1:5 ratio-homogenised dried sample)), was mounted on a double-sided adhesive tape on a metal stub and sputter-coated with a thin coating of gold/palladium (80:20) for 60 s (Quorum SC7620 Sputter Coater) under vacuum. The SEM instrument operating

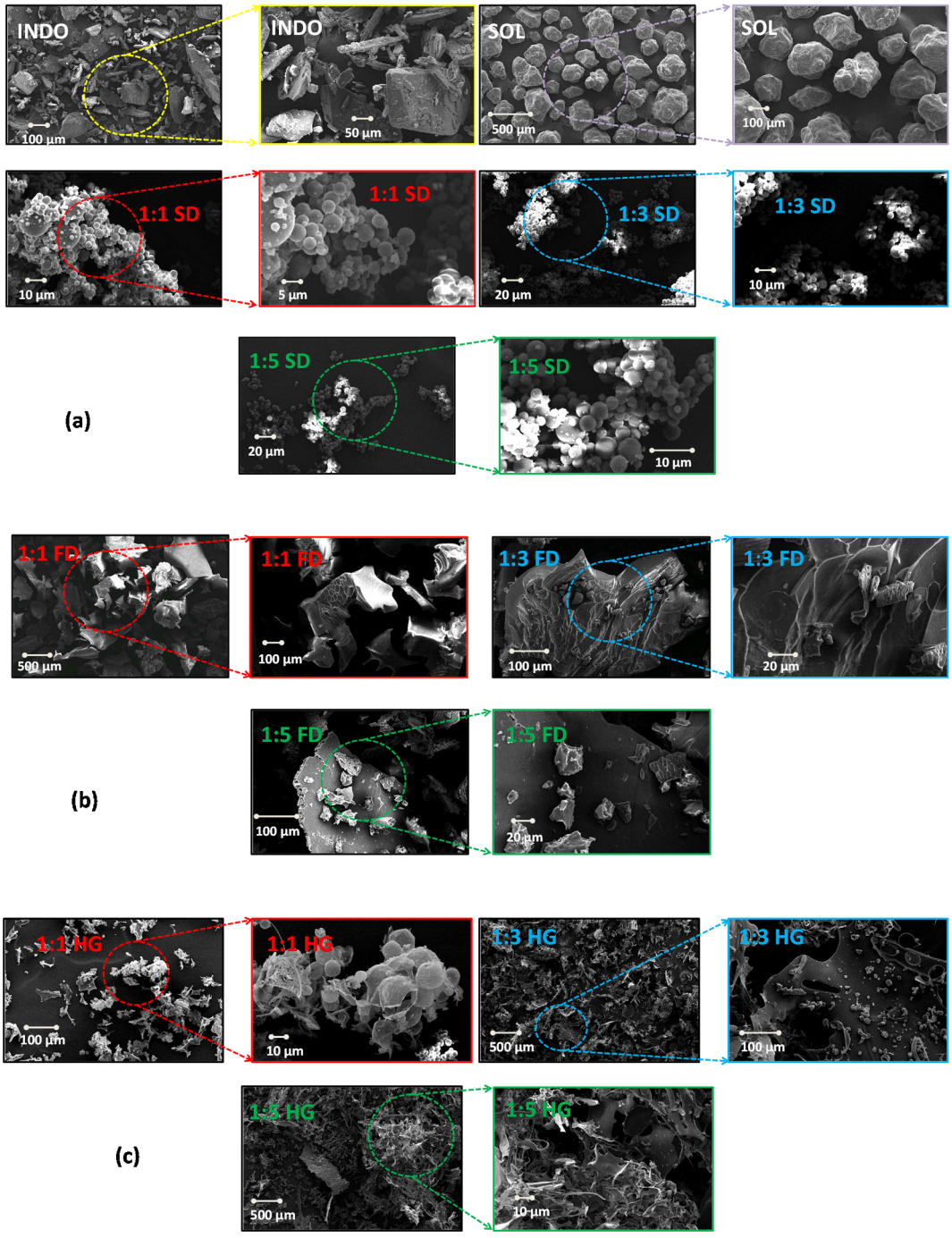

Fig. 6. SEM images for the (a) INDO drug, SOL and the 1:1 SD, 1:3 SD and 1:5 SD dispersions, (b) 1:1 FD, 1:3 FD and 1:5 FD dispersions, (c) 1:1 HG, 1:3 HG and 1:5 HG dispersions.

at 10 kV was used to obtain the electron micrographs. Different magnifications were taken to aid the study of the morphology of the solid dispersions.

2.3.2. *Differential scanning calorimetry (DSC)*

About 5–10 mg of each sample (INDO, SOL, SD1:1 (1:1 ratio-spray dried sample), SD1:3 (1:3 ratio-spray dried sample), SD1:5 (1:5 ratio-spray dried sample), FD1:1 (1:1 ratio-freeze dried sample), FD1:3 (1:3 ratio-freeze dried sample), FD1:5 (1:5 ratio-freeze dried sample), HG1:1 (1:1 ratio-homogenised dried sample), HG1:3 (1:3 ratio- homogenised dried sample) or HG1:5 (1:5 ratio-homogenised dried sample)), was placed in a standard aluminium pan (40 µL) with a vented lid. This was then crimped and heated from 50 to 180 °C at a scanning rate of 10 °C/min with nitrogen gas as the purge gas (DSC1 Mettler-Toledo, Switzerland). The enthalpy, onset temperatures and melting points of the starting materials and the various solid dispersions as well as their glass transition temperatures were analysed using the software provided by Mettler-Toledo, Switzerland.

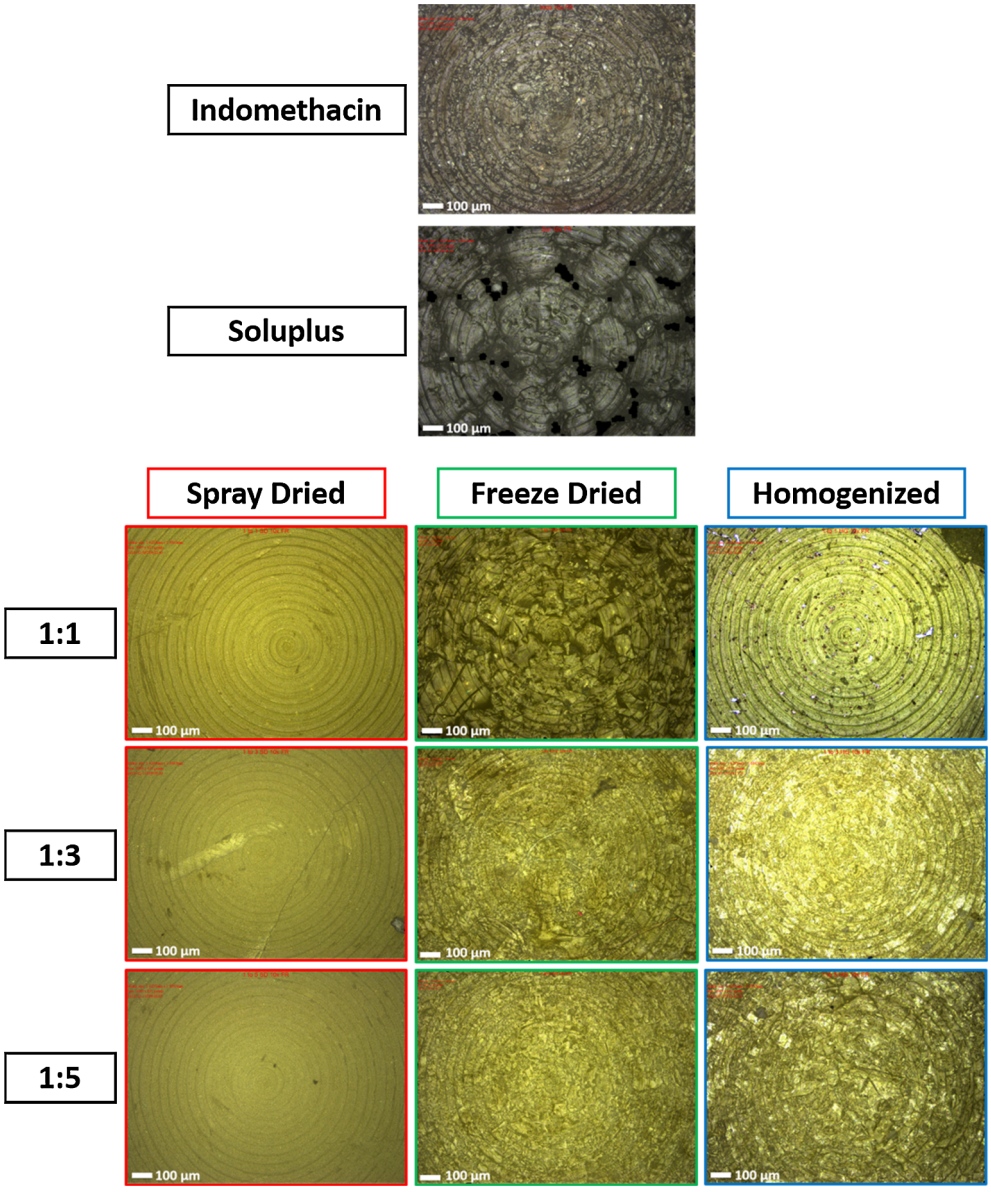

Fig. 7. Focus variation instrument images at 10× magnification of the representative compacts of INDO, SOL and respective solid dispersions. Images highlight impressions from the tooling that could potentially affect IDR measurements. Note: scale bar is 100 µm.

2.3.3. X-ray powder diffraction (XRPD)

The XRPD patterns of each sample (INDO, SOL, SD1:1 (1:1 ratio-spray dried sample), SD1:3 (1:3 ratio-spray dried sample), SD1:5 (1:5 ratio-spray dried sample), FD1:1 (1:1 ratio-freeze dried sample), FD1:3 (1:3 ratio-freeze dried sample), FD1:5 (1:5 ratio-freeze dried sample), HG1:1 (1:1 ratio-homogenised dried sample), HG1:3 (1:3 ratio- homogenised dried sample) and HG1:5 (1:5 ratio-homogenised dried sample)), were scanned in Bragg–Brentano geometry, over a scattering (Bragg, 2θ) angle range from 5 to 100°, in 0.02° steps at 1.5° min^{-1} using a D2 Phaser diffractometer (Bruker AXS GmbH, Karlsruhe, Germany) (Laity et al., 2015). Microsoft Excel was used to analyse the collected XRPD patterns.

2.4. Assay measurements

20 mg of each sample SD1:1 (1:1 ratio-spray dried sample), SD1:3 (1:3 ratio-spray dried sample), SD1:5 (1:5 ratio-spray dried sample), FD1:1 (1:1 ratio-freeze dried sample), FD1:3 (1:3 ratio-freeze dried sample), FD1:5 (1:5 ratio-freeze dried sample), HG1:1 (1:1 ratio-homogenised dried sample), HG1:3 (1:3 ratio- homogenised dried sample) and HG1:5 (1:5 ratio-homogenised dried sample)), was placed into a 100 mL volumetric flask and made up to volume using the pH 7.2 to allow it to dissolve. 1 mL of this dissolved solution was withdrawn using a micropipette and placed into a 10 mL volumetric flask, and made up to volume using the pH 7.2 media. This was carried out in triplicate for each sample. The INDO content in each sample was determined at a wavelength of 320 nm using a Cary 60 UV–Vis spectrophotometer (Agilent Technologies). The concentration of INDO in the various formulations were then calculated after subjecting the absorbance values through an equation of best fit derived from a calibration curve of INDO with an r^2 value of 0.9993.

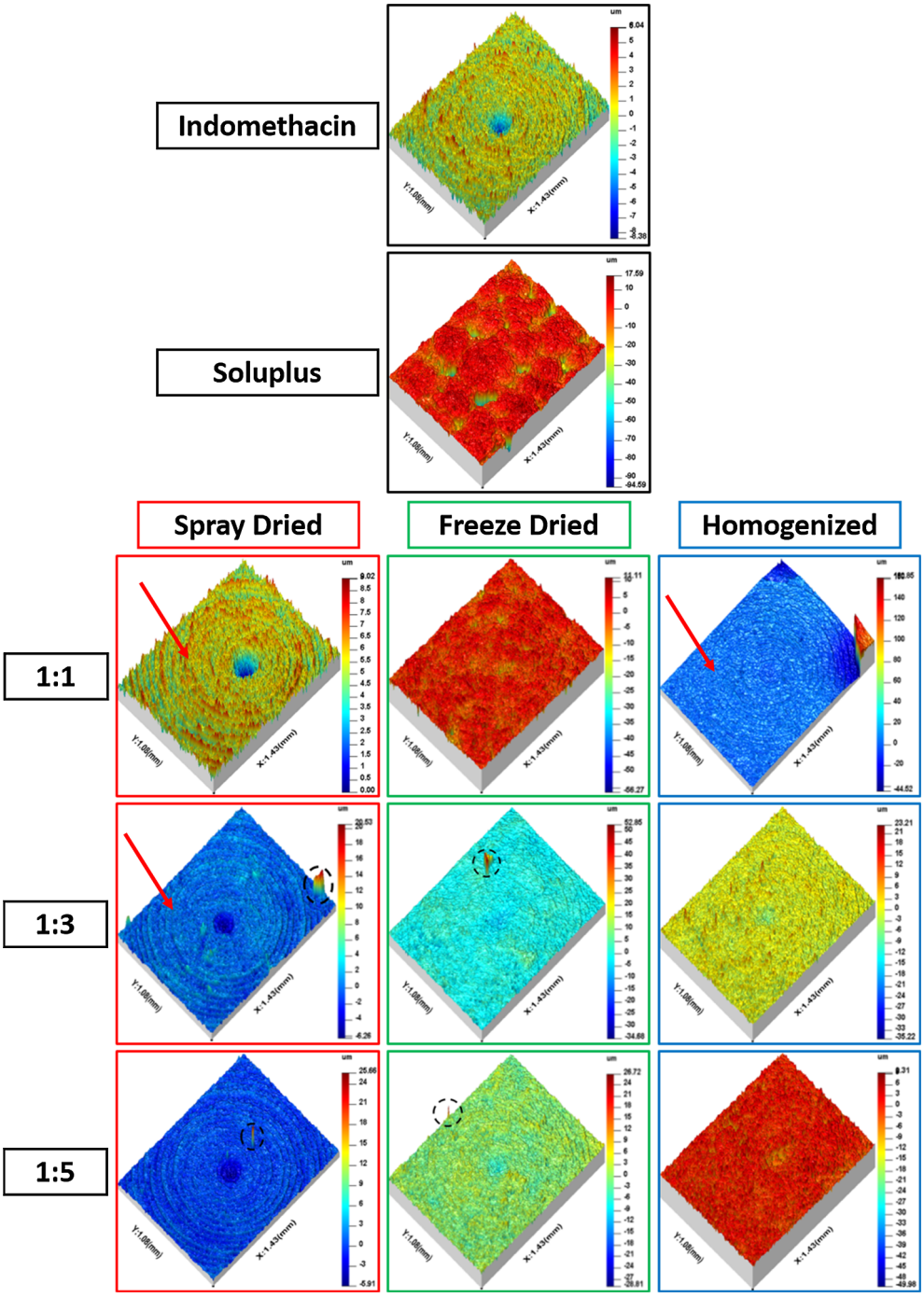

Fig. 8. 3D images of the surface roughness data set gathered from the focus variation instrument of INDO, SOL and the respective solid dispersions. Images shown from 10× magnification to highlight particulates (dashed black circular lines) and impressions from the tooling that could potentially affect IDR measurements.

2.5. Surface analysis of compacts and UV imaging of intrinsic dissolution rate (IDR) and pseudo IDR

Compacts (3 mm) for surface analysis or UV imaging for IDR pseudo IDR were produced by using 10 mg of either INDO, SD1:1 (1:1 ratio-spray dried sample), SD1:3 (1:3 ratio-spray dried sample), SD1:5 (1:5 ratio-spray dried sample), FD1:1 (1:1 ratio-freeze dried sample), FD1:3 (1:3 ratio-freeze dried sample), FD1:5 (1:5 ratio-freeze dried sample), HG1:1 (1:1 ratio-homogenised dried sample), HG1:3 (1:3 ratio-homogenised dried sample) or HG1:5 (1:5 ratio-homogenised dried sample) at a compression force of 100 kg for 1 min using a hand-crank press (Pion Inc). The focus variation microscope Alicona™ microscope (Alicona Imaging GmbH, Graz, Austria) was used for the surface assessment as previously reported by Ward et al., 2017 [41]. The surface assessment of the compacts prior to IDR (INDO drug) or pseudo IDR (for all the formulations made –the same set-up for determining IDR from the parent drug INDO was used in determining the images and values for the solid dispersion samples. This is what the authors are terming

Table 1
Intrinsic dissolution rates (IDR and pseudo IDR), developed interfacial (surface) area ratio (Sdr) and texture aspect ratio (Str) for INDO and the solid dispersions produced from the different preparation methods.

Formulation	IDR (μg/min/cm^2)*	Sdr **(%)	Str**
INDO	59.15 ± 0.23	1.72	0.776
1:1 SD	24.22 ± 0.36***	0.79	0.846
1:3 SD	30.84 ± 0.33***	0.86	0.797
1:5 SD	19.21 ± 0.83***	0.72	0.918
1:1 FD	73.56 ± 1.65***	16.29	0.892
1:3 FD	37.17 ± 0.83***	5.75	0.675
1:5 FD	16.72 ± 0.51***	3.37	0.882
1:1 HG	70.02 ± 9.77***	44.65	0.362
1:3 HG	31.32 ± 3.96***	5.84	0.883
1:5 HG	32.71 ± 13.86***	9.14	0.804

Note: * depicts n = 3 experiments, **depicts n = 10 experiments, and *** depicts pseudo IDR values.

"pseudo IDR") determination allowed the effect of the preparation method (spray drying, freeze drying and homogenising) of the solid dispersions on the developed interfacial (surface) area ratio (Sdr) to be determined over that of the parent drug INDO. The true surface area of the textured sample compared to that of a uniform flat surface of equal size is known as the Sdr. It is expressed as a percentage by which the true measured surface area exceeds that of the nominal uniform measurement area (Eq. (1)) allowing for a surface gain to be calculated. The texture aspect ratio parameter (Str) was used to assess the uniformity of the texture of the compacts for IDR or pseudo IDR determination. The area used in determining the Sdr and Str is depicted in Fig. 1. The closer to 1 the Str value lies, the more uniform the surface is, whereas the closer to 0 the value is, the more likely a dominant texture direction is influencing the surface. This is in line with guidance described in ISO 25,178 [47]. The Surfstand™ software (Taylor Hobson, UK, and University of Huddersfield, UK) was used to analyse the acquired focus variation images to produce the 3D roughness maps in order to generate the values for both Sdr and Str.

$$Sdr = \frac{(Texture\ \ Surface\ \ Area) - (Cross\ \ Sectional\ \ Area)}{Cross\ \ Sectional\ \ Area} \quad (1)$$

The SDI2 flow through cell (Pion Inc) was then used in the determination of IDR or pseudo IDR (Fig. 2a). The same compacts that were made and assessed for their surface texture was used for IDR determination. This allowed the authors to determine if the surfaces impacted IDR or pseudo IDR measurements. Fig. 2a displays the flow through set-up for IDR or pseudo IDR determination with a key explaining the various components involved. Fig. 2b shows an example of the images that are produced from such analysis indicating the direction of flow, compact location, drug dissolution and where the drug measurement zone is. The molar extinction coefficient of INDO was experimentally determined by using a concentrations range of 2.8×10^{-6} to 1.4×10^{-4} mol/L. The range of concentrations used was within the linear region and produced an r^2 value of 0.999. All experiment were conducted in triplicates. pH 7.2 was used as the dissolution medium at a flow rate of 2 mL/min for 30 min at 37 °C. All experiments were conducted in triplicate and at a wavelength of 320 nm.

2.6. UV imaging and dissolution of whole dosage form

The schematic of how the whole dosage form cell (which is the additional capability of the new SDI2) operates is depicted in Fig. 3a. Fig. 3b shows an example of the images that are generated from whole dose analysis indicating the direction of flow, wire holder, whole dosage form, drug dissolution and where the drug measurement zone is. Capsules containing 2.5 mg of INDO or 2.5 mg INDO content determined from the assay measurements in Section 2.4 from SD1:1 (1:1 ratio-spray dried sample), SD1:3 (1:3 ratio-spray dried sample), SD1:5 (1:5 ratio-spray dried sample), FD1:1 (1:1 ratio-freeze dried sample), FD1:3 (1:3 ratio-freeze dried sample), FD1:5 (1:5 ratio-freeze dried sample), HG1:1 (1:1 ratio-homogenised dried sample), HG1:3 (1:3

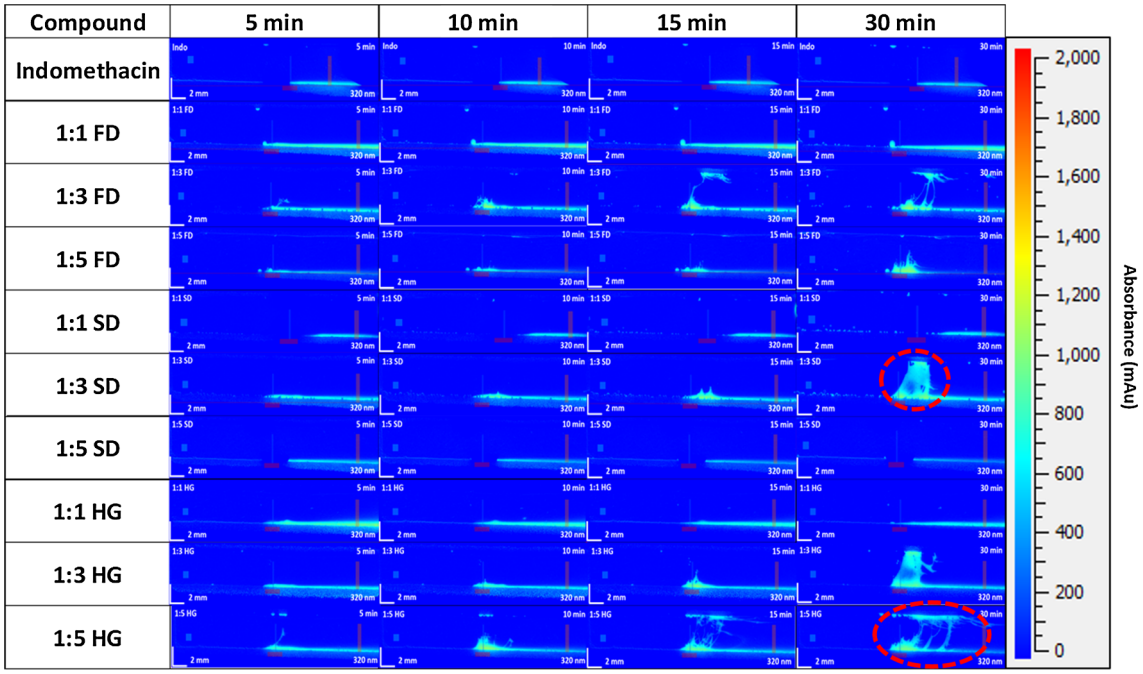

Fig. 9. Surface dissolution imaging of INDO and the 1:1 SD, 1:3 SD, 1:5 SD, 1:1 FD, 1:3 FD, 1:5 FD, 1:1 HG, 1:3 HG and 1:5 HG dispersions at the 5, 10, 15 and 30 min time points. A red circle depicts the "web-like" development that may have resulted in decreases/increases in IDR values for some of the solid dispersions. *Note:* scale bar is 2 mm. (For interpretation of the references to colour in this figure legend, the reader is referred to the web version of this article.)

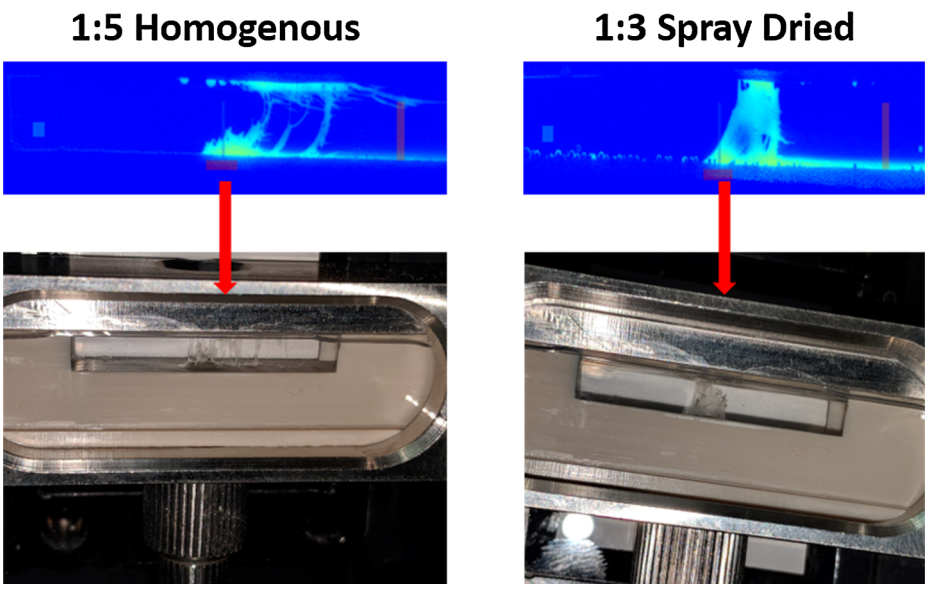

Fig. 10. Images captured of the web-like phenomenon within the IDR flow through cell taking place in the UV experiments.

ratio- homogenised dried sample) or HG1:5 (1:5 ratio-homogenised dried sample) were prepared using a size 0 hard gelatine capsules. These samples were then mounted using a wire holder and placed within the sample holder. The whole dosage cell with glass beads added was inserted and connected to the fluid lines. The experiment was conducted using pH 7.2 at a flow rate of 8.2 mL/min at 37 °C. The release of INDO and the various solid dispersions prepared from the different techniques was imaged over 60 min at various time points at a wavelength of 320 nm. All experiments were conducted in triplicate.

3. Results and discussion

3.1. Solid-state analysis

XRPD was used to confirm the nature of the prepared solid dispersion samples as well as the nature and starting polymorph of INDO. This analysis was conducted straight after sample preparation. The obtained XRPD patterns are depicted in Fig. 4. Characteristic peaks of the samples were confirmed by the differences in the diffraction pattern between 5° and 40° 2θ. Characteristic peaks at 11.6, 16.8, 19.6, and 26.6° 2θ suggest INDO was the γ-polymorph [17,48]. It was also evident from the diffractions that SOL was fully amorphous with no distinct crystalline peaks. The XRPD pattern in Fig. 4a–c indicated that regardless of the preparation method (spray drying, freeze drying and homogenisation) of solid dispersions, the resultant products were all in the amorphous state. The diffused halo diffraction pattern present therefore suggests that the crystalline INDO was molecularly dispersed within the SOL. This may potentially have implications on the pseudo IDR and dissolution rate of INDO in the solid dispersions. The XRD patterns of all the produced solid dispersions were assessed after a year of storage and were all found to be still amorphous (Supplementary material S1).

The DSC thermograms of INDO, SOL, and the produced solid dispersions from the three different preparation methods are depicted in Fig. 5. The sharp endothermic peak exhibited by INDO on the DSC at 161.98 °C corresponds to its melting point and confirmed the γ polymorphic nature of INDO [28,49]. Fig. 5 shows SOL is amorphous with a glass transition around 70 °C [50]. It was interesting to note also that the peak corresponding to INDO's melting point at 161.98 °C was absent in all the solid dispersions (SD, FD and HG samples), further reinstating its amorphous state and confirming that INDO was molecularly dispersed in SOL. The glass transition temperature in the 1:1 SD (58.82 °C), 1:3 SD (60.26 °C), 1:5 SD (63.61 °C), 1:1 FD (60.82 °C), 1:3 FD (58.98 °C), 1:5 FD (50.61 °C), 1:1 HG (48.13 and 66.33 °C), 1:3 HG (67.15 °C) and 1:5 FD (68.60 °C) samples was further proof of their amorphous state. This therefore showed that the addition of SOL to INDO using the various preparation techniques inhibited the crystallisation of INDO. XRPD and DSC thus proved complimentary in determining the state of INDO in the solid dispersions.

SEM images of INDO, SOL and the various solid dispersion samples are depicted in Fig. 6. The SEM images showed marked differences in the morphology and microstructure between the samples produced by SD, FD and HG techniques. All particles prepared by the three preparation methods had variable shapes and sizes. The SD process yielded spherical particles. The size of the obtained particles remained fairly consistent and uniform with the particles clustering together (Fig. 6a). It was interesting to note that despite the FD and HG samples being subjected to the freeze drying process, they had different morphologies. The FD dispersions appeared to be highly porous with wrinkled surfaces and a relatively complex structure (Fig. 6b). The HG samples however appeared to have no real structure to them with varied particle sizes (Fig. 6c). This could be attributed to the homogenising process and could potentially have an effect on pseudo IDR and dissolution.

3.2. Intrinsic dissolution rate

Ward et al., 2017 [41] used a focus variation microscope to show uneven and loose particulates on the surfaces of compacts ready for IDR UV imaging can give rise to erroneous data. This had been observed previously by Niederquell and Kuentz 2014 [32] using SEM. As the surface integrity of compact has been proven to be important [16], the surfaces of all compacts were extensively studied at 10× magnifications on the focus variation instrument (as in schematic for Fig. 1). The 2D images in Fig. 7 at the 10× magnification show that all the samples (SD, FD and HG and the pure drug INDO) picked up the "rings" on the tooling surface. It was interesting to note also that the morphology of the SEM image of SOL (Fig. 6a) was picked up on the compact surface (Fig. 7). Fig. 7 shows a nice uniform surface produced from the spherical particles produced from the spray drying process. The

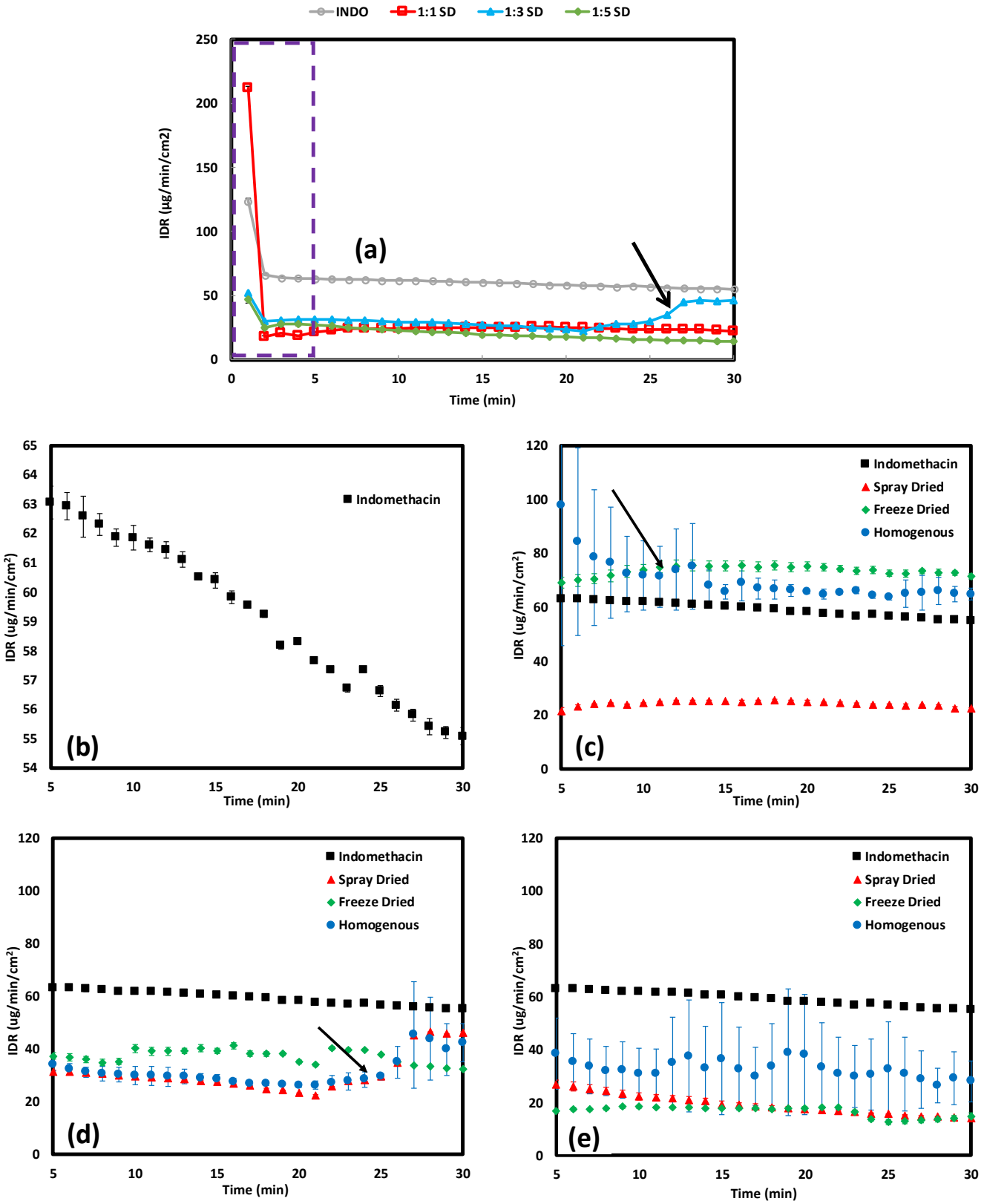

Fig. 11. IDR or "pseudo" IDR as a function of time for the (a) INDO and spray dried formulations only. The purple inserts elaborates the relatively higher IDR or "pseudo" IDR values at the earlier time points which may be due to drug or solid dispersion dust particulates being on the surfaces of the compacts. (b) IDR for INDO (c) 1:1 SD, 1:1 FD and 1:1 HG (d) 1:3 SD, 1:3 FD and 1:3 HG (e) 1:5 SD, 1:5 FD and 1:5 HG dispersions. The black arrows indicate increases/decreases in IDR or "pseudo" IDR at those time points possibly due to the behaviour of the dispersions as in Figs. 9 and 10. Note: IDR data was reported after the 5 min mark only for b–e. *Note:* where standard deviations are not seen is because they are smaller than the marker. (For interpretation of the references to colour in this figure legend, the reader is referred to the web version of this article.)

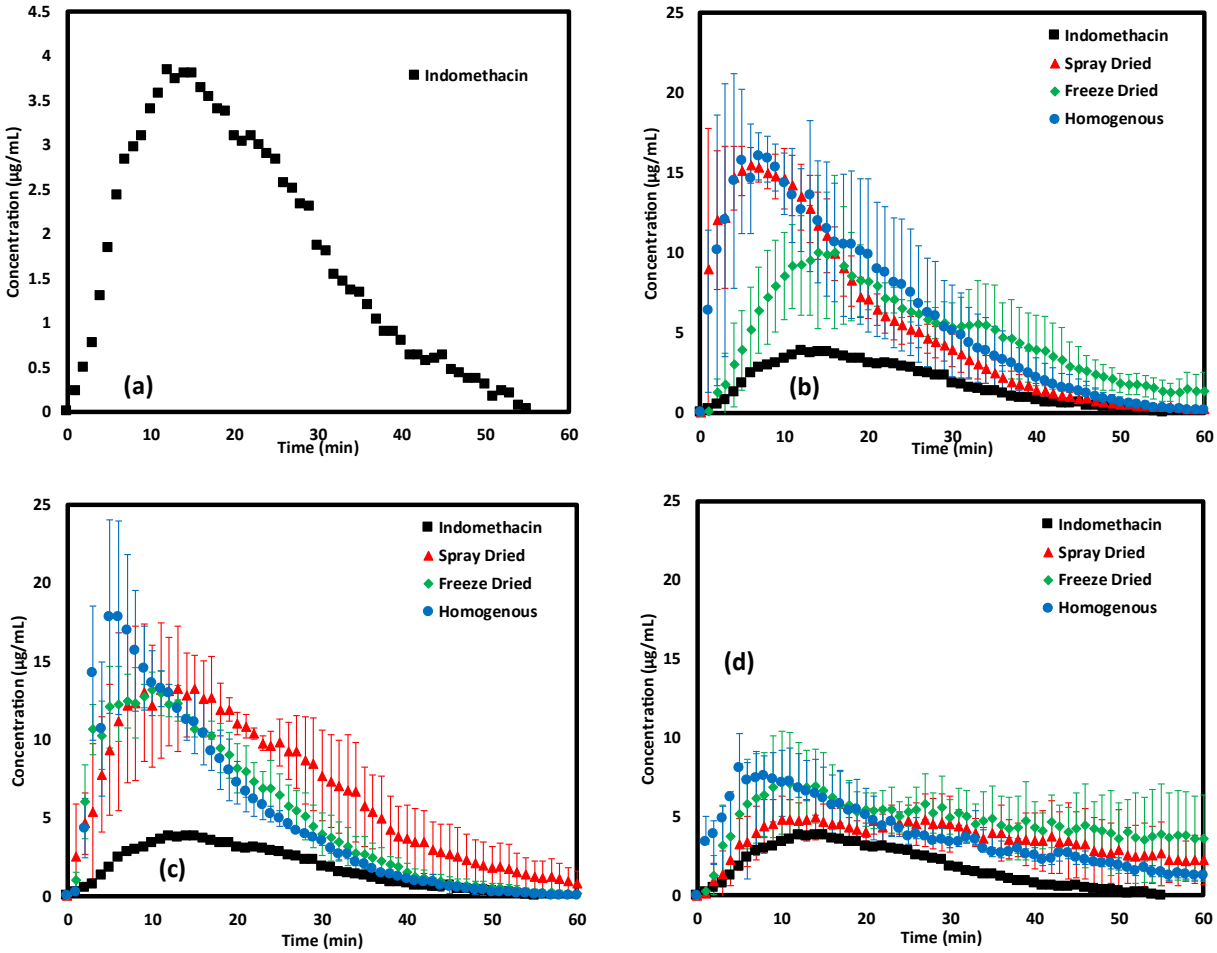

Fig. 12. Amount of (a) INDO (b) 1:1 SD, 1:1 FD and 1:1 HG dispersions, (c) 1:3 SD, 1:3 FD and 1:3 HG dispersions, (d) 1:5 SD, 1:5 FD and 1:5 HG dispersions released over 60 min using the whole dosage cell. *Note:* where standard deviations are not seen is because they are smaller than the marker.

complimentary Surfstand™ 3D images of the compacts in Fig. 8 confirm changes in the surface parameters from INDO to the various formulations. Surfstand analysis of the INDO compact showed it had an Sdr (represented as a percentage) gain of 1.72% at the 10× magnification. The Sdr value indicates the surface area gained as a result of the texture of the samples. It was interesting to observe how a change in the morphology affected the Sdr. The spray dried dispersions had the lowest surface gain (even lower than the INDO drug) for all the samples with the homogenised samples having the highest gains (Table 1) which may be due to the way the particles pack and compact due to their morphologies. Compression lines from the tooling can also be seen in these images (as indicated by the red arrows) as well as powder particulates (indicated by the black dashed circles) which may have implications on IDR determination. Hulse et al., 2012 [36] therefore reported using IDR values after the 3 min mark from a UV imaging technique due to potential erroneous measurements as a result of drug particles on the surface. IDR results here (Table 1) are reported from the 5 min time point as reported in Asare-Addo et al., 2018 [16]. Another interesting observation was that there was a uniformity of texture (Str) for all the samples with the exception of the 1:1 homogenised samples which coincidently had the highest Sdr also (Table 1).

The UV images from IDR determination of INDO and pseudo IDR determination from the solid dispersion samples are shown in Fig. 9. Fig. 9 showed some interesting phenomenon occurring for some of the solid dispersions which we believe we are reporting for the first time. The red dashed lines show “web like” strands produced during the pseudo IDR run. These seem to be generally prominent with increased SOL content in the solid dispersions. This is also visualised in the flow through cell taken out after the pseudo IDR run in the images depicted in Fig. 10. The authors believe this to be a viscosity phenomenon due to the increased polymer levels. To rule out possible interactions or complexations, the authors have exploited isothermal calorimetry and additional pseudo IDR runs with the pure SOL, spray dried SOL, freeze dried SOL and various combinations with pure INDO (Supplementary material S2, S3 and S4). The IDR and pseudo IDR figures and values are depicted in Fig. 11 and Table 1. These IDR and pseudo IDR values were obtained from the use of the molar extinction coefficient value ($9590.5\ M^{-1}\ cm^{-1}$) obtained from the INDO concentration ranges explored from Section 2.5. The black arrows in Fig. 11 indicate increases/decreases in pseudo IDR at those time points possibly due to the behaviour of the compacts described (Fig. 9). This visual way of determining IDR thus highlights the importance of this UV imaging technique in generating IDR or pseudo IDR values as it gives a visual into drug behaviour thereby allowing a formulator to give consideration to data gathered in the decision process. All the spray dried solid dispersions showed a significant decrease in the pseudo IDR values compared to the IDR of INDO (Table 1). The 1:1 FD and HG samples both had improvement in their pseudo IDR values over the parent drug INDOs IDR. Both the 1:3 and 1:5 samples for the FD and HG samples however had lower pseudo IDR values than the IDR of INDO (Table 1)

Fig. 13. Gel layer on remaining capsule after 60 min UV dissolution imaging. This was characteristic for the 1:5 SD, FD and HG samples.

suggesting freeze drying and homogenising at the 1:1 INDO:SOL ratio to be best candidates in improving the IDR of INDO. These mixed results maybe a combination of several factors that includes microstructure, viscosity at the surface of the compacts and solid fraction effects on samples. The INDO compacts were analysed using XRPD post IDR run was found to in the γ-polymorph form (Supplementary material S5) [17,48].

3.3. Whole dosage form imaging

Assaying all the formulations produced allowed accurate determinations of drug content in the various ratios of the solid dispersions. Fig. 12 shows the release as determined from the UV imaging of the INDO, SD, FD and HG solid dispersions. INDO had an average concentration of 1.62 ± 0.001 μg/mL over the 60 min period. The 1:1 SD, 1:3 SD and 1:5 SD had average concentrations of 5.42 ± 1.12 μg/mL, 6.62 ± 2.3 μg/mL and 3.53 ± 1.45 μg/mL respectively. The 1:1 FD, 1:3 FD and 1:5 FD had average concentrations of 4.78 ± 1.82 μg/mL, 5.04 ± 0.94 μg/mL and 4.73 ± 2.08 μg/mL respectively. The 1:1 HG, 1:3 HG and 1:5 HG had average concentrations of 6.07 ± 2.45 μg/mL, 5.00 ± 1.08 μg/mL and 3.79 ± 1.01 μg/mL respectively. All the solid dispersions showed improvements in the average concentrations of INDO content over the parent or untreated INDO. This did not correlate in any way with the pseudo IDR data which showed two samples only to increase the dissolution rate over that of the parent drug INDO thereby highlighting the importance of using both imaging techniques. The authors suggest the behaviour of the compacts (contribution of SOL) as imaged in Fig. 9 to be responsible for the low pseudo IDR values experienced in the amorphous solid dispersions. The “lower” average concentration values for all the 1:5 INDO to SOL ratio samples was attributed to the gel like-layer (Fig. 13) that had formed around the sample due to the higher SOL content after capsule shell dissolution. This gel layer may have increased the diffusion pathway for INDO dissolution [51,52]. The area under the curve suggests the best five samples dissolution wise to be 1:3 SD > 1:1 HG > 1:1 SD > 1:3 FD > 1:3 HG. This means that a ratio of INDO to SOL in these dispersions of up to 1:3 is sufficient to produce significant dissolution increases. The authors have also for the first time according to our knowledge used this UV imaging technique to capture the dissolution of a capsule with its tip coming off over time to allow drug into the media (Fig. 14). The full dosage imaging is also presented in Fig. 15. These images allow a quick visualisation of the processes that yielded Fig. 12. The 1:1 SD, 1:1 HG and 1:3 HG for example shows the quick saturation of the INDO in the image and this is represented in Fig. 12b and c. Again the poor solubility of INDO can be seen in the images as there was hardly any drug dissolved.

4. Conclusion

Successful solid dispersion formulations of INDO and SOL were made at three ratios (1:1, 1:3 and 1:5 (drug:SOL)) using three manufacturing techniques. These were spray drying, freeze drying and homogenising. These solid dispersions were fully characterised and confirmed as being amorphous using DSC and XRPD. Pseudo IDR determined using a UV imaging technique set-up for IDR determinations deduced only two samples to have superior pseudo IDR values to the

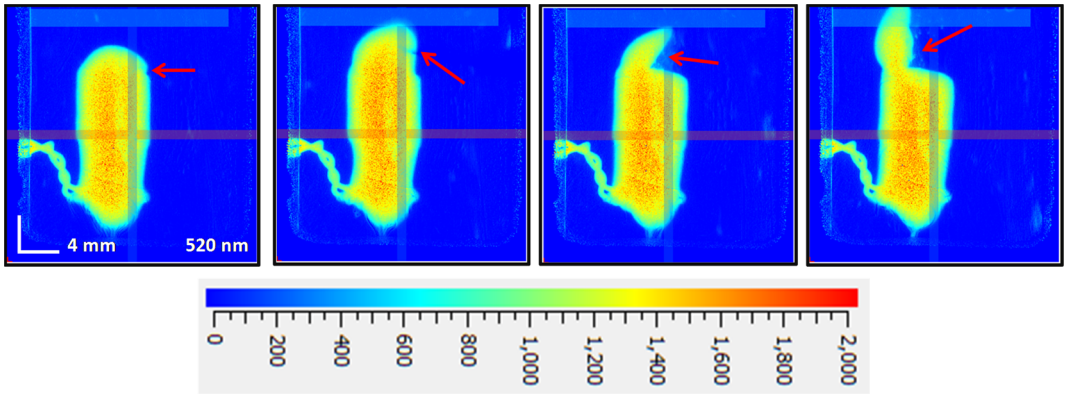

Fig. 14. Full dosage imaging of a capsule. Red arrows indicate how the tip of the capsule comes off with time to allow the drug to go in solution. *Note:* scale bar is 4 mm. (For interpretation of the references to colour in this figure legend, the reader is referred to the web version of this article.)

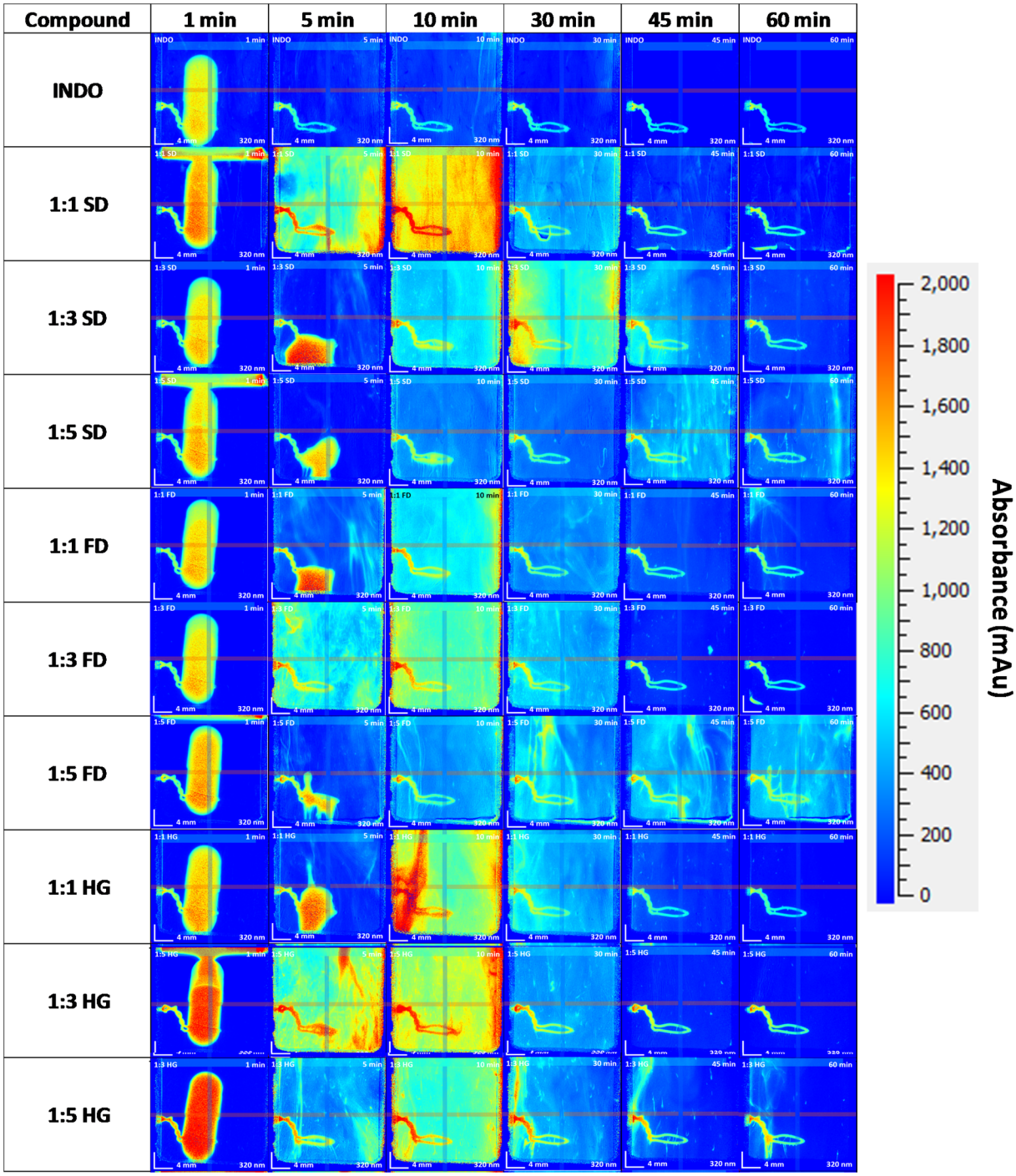

Fig. 15. Full dosage imaging of (a) INDO and the 1:1 SD, 1:3 SD, 1:5 SD, 1:1 FD, 1:3 FD, 1:5 FD, 1:1 HG, 1:3 HG and 1:5 HG dispersions at the 1, 5, 10, 15, 30, 45 and 60 min. *Note:* Samples were imaged over a 60 min period. Note: scale bar is 4 mm.

IDR of the parent drug INDO. The IDR and pseudo IDR UV images showed a phenomenon the authors are reporting for the first time where increased polymer content produced "web-like" strands that migrated to the top of the quartz cell which may have caused the decrease in the pseudo IDR values for the solid dispersions. The whole dose imaging (capsule) showed all the samples (spray drying, freeze drying and homogenising) had superior dissolution to that of the parent drug INDO. The area under the curve suggested the best five samples dissolution wise to be 1:3 SD > 1:1 HG > 1:1 SD > 1:3 FD > 1:3 HG meaning a ratio of INDO to SOL in these dispersion of up to 1:3 was sufficient to produce significant dissolution increases. As such a formulators choice of instrumentation/techniques to use may well come down to cost or instrument availability. This work highlighted the importance of having both complimentary IDR and whole dosage imaging techniques in giving a better understanding of solid dispersion systems.

Acknowledgements

The authors would like to acknowledge the University of Huddersfield for financial support. The authors also acknowledge Breeze Outwaite, Hayley Watson, Paul Whittles and Karl Box all of Pion Inc, UK for their technical expertise on the use of the SDI2 instrument.

Appendix A. Supplementary material

Supplementary data to this article can be found online at https://doi.org/10.1016/j.ejpb.2019.03.002.

References

[1] N. Kanikkannan, Technologies to improve the solubility, dissolution and bioavailability of poorly soluble drugs, J. Anal. Pharm. Res. 7 (2018) 1–7, https://doi.org/10.15406/japlr.2018.07.00198.
[2] M.G. Papich, M.N. Martinez, Applying Biopharmaceutical Classification System (BCS) criteria to predict oral absorption of drugs in dogs: challenges and pitfalls, AAPS J. 17 (2015) 948–964, https://doi.org/10.1208/s12248-015-9743-7.
[3] P. Khadka, J. Ro, H. Kim, I. Kim, J.T. Kim, H. Kim, J.M. Cho, G. Yun, J. Lee, Pharmaceutical particle technologies: An approach to improve drug solubility, dissolution and bioavailability, Asian J. Pharm. Sci. 9 (2014) 304–316, https://doi.org/10.1016/j.ajps.2014.05.005.
[4] G.L. Amidon, H. Lennernäs, V.P. Shah, J.R. Crison, A theoretical basis for a biopharmaceutic drug classification: the correlation of in vitro drug product dissolution and in vivo bioavailability, Pharm. Res. 12 (1995) 413–420, https://doi.org/10.1023/A:1016212804288.
[5] C. Leuner, J. Dressman, Improving drug solubility for oral delivery using solid dispersions, Eur. J. Pharm. Biopharm. 50 (2000) 47–60, https://doi.org/10.1016/S0939-6411(00)00076-X.
[6] A.O. Adebisi, W. Kaialy, T. Hussain, H. Al-Hamidi, A. Nokhodchi, B.R. Conway, K. Asare-Addo, An assessment of triboelectrification effects on co-ground solid dispersions of carbamazepine, Powder Technol. 292 (2016), https://doi.org/10.1016/j.powtec.2016.02.008.
[7] A.O. Adebisi, W. Kaialy, T. Hussain, H. Al-Hamidi, A. Nokhodchi, B.R. Conway, K. Asare-Addo, Solid-state, triboelectrostatic and dissolution characteristics of spray-dried piroxicam-glucosamine solid dispersions, Colloids Surfaces B Biointerfaces 146 (2016) 841–851, https://doi.org/10.1016/J.COLSURFB.2016.07.032.
[8] H. Al-Hamidi, K. Asare-Addo, S. Desai, M. Kitson, A. Nokhodchi, The dissolution and solid-state behaviours of coground ibuprofen–glucosamine HCl, Drug Dev. Ind. Pharm. (2014) 1–11, https://doi.org/10.3109/03639045.2014.991401.
[9] E. Šupuk, M.U. Ghori, K. Asare-Addo, P.R. Laity, P.M. Panchmatia, B.R. Conway, The influence of salt formation on electrostatic and compression properties of flurbiprofen salts, Int. J. Pharm. 458 (2013) 118–127, https://doi.org/10.1016/j.ijpharm.2013.10.004.
[10] M. Ramirez, S.E. David, C.H. Schwalbe, K. Asare-Addo, B.R. Conway, P. Timmins, Crystal packing arrangement, chain conformation, and physicochemical properties of gemfibrozil amine salts, Cryst. Growth Des. 17 (2017) 3743–3750, https://doi.org/10.1021/acs.cgd.7b00352.
[11] E. Pindelska, A. Sokal, W. Kolodziejski, Pharmaceutical cocrystals, salts and polymorphs: advanced characterization techniques, Adv. Drug Deliv. Rev. 117 (2017) 111–146, https://doi.org/10.1016/J.ADDR.2017.09.014.
[12] S.E. David, P. Timmins, B.R. Conway, Impact of the counterion on the solubility and physicochemical properties of salts of carboxylic acid drugs, Drug Dev. Ind. Pharm. 38 (2012) 93–103, https://doi.org/10.3109/03639045.2011.592530.
[13] H. Al-Hamidi, A.A. Edwards, D. Douroumis, K. Asare-Addo, A.M. Nayebi, S. Reyhani-Rad, J. Mahmoudi, A. Nokhodchi, Effect of glucosamine HCl on dissolution and solid state behaviours of piroxicam upon milling, Colloids Surf B 103 (2013) 189–199, https://doi.org/10.1016/j.colsurfb.2012.10.023.
[14] H. Al-Hamidi, A.A. Edwards, M.A. Mohammad, A. Nokhodchi, Glucosamine HCl as a new carrier for improved dissolution behaviour: Effect of grinding, Colloids SurfB 81 (2010) 96–109, https://doi.org/10.1016/j.colsurfb.2010.06.028.
[15] H. Al-Hamidi, A.A. Edwards, M.A. Mohammad, A. Nokhodchi, To enhance dissolution rate of poorly water-soluble drugs: Glucosamine hydrochloride as a potential carrier in solid dispersion formulations, Colloids SurfB 76 (2010) 170–178, https://doi.org/10.1016/j.colsurfb.2009.10.030.
[16] K. Asare-Addo, K. Walton, A. Ward, A.M. Totea, S. Taheri, M. Alshafiee, N. Mawla, A. Bondi, W. Evans, A. Adebisi, B.R. Conway, P. Timmins, Direct imaging of the dissolution of salt forms of a carboxylic acid drug, Int. J. Pharm. 551 (2018) 290–299, https://doi.org/10.1016/j.ijpharm.2018.09.048.
[17] K. Asare-Addo, E. Šupuk, H. Al-Hamidi, S. Owusu-Ware, A. Nokhodchi, B.R. Conway, Triboelectrification and dissolution property enhancements of solid dispersions, Int. J. Pharm. 485 (2015) 306–316, https://doi.org/10.1016/j.ijpharm.2015.03.013.
[18] A. Nokhodchi, Y. Javadzadeh, M.B.-J.M. Siahi-Shadbad, The effect of type and concentration of vehicles on the dissolution rate of Compacts., poorly soluble drug (indomethacin) from liquisolid, J. Pharm. Pharm. Sci. 8 (2005) 18–25.
[19] B.E. Rabinow, Nanosuspensions in drug delivery, Nat. Rev. Drug Discov. 3 (2004) 785–796, https://doi.org/10.1038/nrd1494.
[20] P.H. Stahl, C.G. Wermuth, International Union of Pure and Applied Chemistry., Handbook of pharmaceutical salts: properties, selection, and use, 2008. www.iupac.org/publications/books/author/%0Ahttps://books.google.com/books?id=IvSEXUZUON8C&pg=PA92&dq=%22free+acid%22+salt&hl=en&sa=X&redir_esc=y#v=onepage&q=%22free acid%22 salt&f=false.
[21] A. Smeets, R. Koekoekx, C. Clasen, G. Van den Mooter, Amorphous solid dispersions of darunavir: Comparison between spray drying and electrospraying, Eur. J. Pharm. Biopharm. 130 (2018) 96–107, https://doi.org/10.1016/j.ejpb.2018.06.021.
[22] R.N. Shamma, M. Basha, Soluplus®: A novel polymeric solubilizer for optimization of Carvedilol solid dispersions: Formulation design and effect of method of preparation, Powder Technol. 237 (2013) 406–414, https://doi.org/10.1016/j.powtec.2012.12.038.
[23] M. Otsuka, Y. Maeno, T. Fukami, M. Inoue, T. Tagami, T. Ozeki, Solid dispersions of efonidipine hydrochloride ethanolate with improved physicochemical and pharmacokinetic properties prepared with microwave treatment, Eur. J. Pharm. Biopharm. 108 (2016) 25–31, https://doi.org/10.1016/j.ejpb.2016.08.008.
[24] A. Homayouni, F. Sadeghi, J. Varshosaz, H.A. Garekani, A. Nokhodchi, Comparing various techniques to produce micro/nanoparticles for enhancing the dissolution of celecoxib containing PVP, Eur. J. Pharm. Biopharm. 88 (2014) 261–274, https://doi.org/10.1016/J.EJPB.2014.05.022.
[25] S.A. Mogal, P.N. Gurjar, D.S. Yamgar, A.C. Kamod, Solid dispersion technique for improving solubility of some poorly soluble drugs, Der Pharm. Lett. 4 (2012) 1574–1586, https://doi.org/10.1016/S0091-679X(06)81022-8.
[26] L.P. Ruan, B.Y. Yu, G.M. Fu, D.N. Zhu, Improving the solubility of ampelopsin by solid dispersions and inclusion complexes, J. Pharm. Biomed. Anal. 38 (2005) 457–464, https://doi.org/10.1016/j.jpba.2005.01.030.
[27] D.N. Nguyen, L. Palangetic, C. Clasen, G. Van Den Mooter, One-step production of darunavir solid dispersion nanoparticles coated with enteric polymers using electrospraying, J. Pharm. Pharmacol. 68 (2016) 625–633, https://doi.org/10.1111/jphp.12459.
[28] N. Ogawa, T. Hiramatsu, R. Suzuki, R. Okamoto, K. Shibagaki, K. Fujita, C. Takahashi, Y. Kawashima, H. Yamamoto, Improvement in the water solubility of drugs with a solid dispersion system by spray drying and hot-melt extrusion with using the amphiphilic polyvinyl caprolactam-polyvinyl acetate-polyethylene glycol graft copolymer and D-mannitol, Eur. J. Pharm. Sci. 111 (2018) 205–214, https://doi.org/10.1016/j.ejps.2017.09.014.
[29] T. Van Duong, G. Van den Mooter, The role of the carrier in the formulation of pharmaceutical solid dispersions. Part II: amorphous carriers, Expert Opin. Drug Deliv. 13 (2016) 1681–1694, https://doi.org/10.1080/17425247.2016.1198769.
[30] K. Kawakami, K. Sato, M. Fukushima, A. Miyazaki, Y. Yamamura, S. Sakuma, Phase separation of supersaturated solution created from amorphous solid dispersions: Relevance to oral absorption, Eur. J. Pharm. Biopharm. 132 (2018) 146–156, https://doi.org/10.1016/j.ejpb.2018.09.014.
[31] X.Y. Lawrence, A.S. Carlin, G.L. Amidon, A.S. Hussain, Feasibility studies of utilizing disk intrinsic dissolution rate to classify drugs, Int. J. Pharm. 270 (1–2) (2004) 221–227.
[32] A. Niederquell, M. Kuentz, Biorelevant dissolution of poorly soluble weak acids studied by UV imaging reveals ranges of fractal-like kinetics, Int. J. Pharm. 463 (2014) 38–49, https://doi.org/10.1016/j.ijpharm.2013.12.049.
[33] J.P. Boetker, J. Rantanen, T. Rades, A. Müllertz, J. Østergaard, H. Jensen, A new approach to dissolution testing by UV imaging and finite element simulations, Pharm. Res. 30 (2013) 1328–1337, https://doi.org/10.1007/s11095-013-0972-0.
[34] S. Gordon, K. Naelapää, J. Rantanen, A. Selen, A. Müllertz, J. Ostergaard, Real-time dissolution behavior of furosemide in biorelevant media as determined by UV imaging, Pharm. Dev. Technol. 18 (2013) 1407–1416, https://doi.org/10.3109/10837450.2012.737808.
[35] L.H. Nielsen, S. Gordon, J.P. Pajander, J. Østergaard, T. Rades, A. Müllertz, Biorelevant characterisation of amorphous furosemide salt exhibits conversion to a furosemide hydrate during dissolution, Int. J. Pharm. 457 (2013) 14–24, https://doi.org/10.1016/j.ijpharm.2013.08.029.
[36] W.L. Hulse, J. Gray, R.T. Forbes, A discriminatory intrinsic dissolution study using UV area imaging analysis to gain additional insights into the dissolution behaviour of active pharmaceutical ingredients, Int. J. Pharm. 434 (2012) 133–139, https://doi.org/10.1016/j.ijpharm.2012.05.023.
[37] N. Qiao, K. Wang, W. Schlindwein, A. Davies, M. Li, In situ monitoring of carbamazepine–nicotinamide cocrystal intrinsic dissolution behaviour, Eur. J. Pharm. Biopharm. 83 (2013) 415–426, https://doi.org/10.1016/J.EJPB.2012.10.005.
[38] J. Østergaard, E. Meng-Lund, S.W. Larsen, C. Larsen, K. Petersson, J. Lenke, H. Jensen, Real-time UV imaging of nicotine release from transdermal patch, Pharm. Res. 27 (2010) 2614–2623, https://doi.org/10.1007/s11095-010-0257-9.
[39] J. Østergaard, J.X. Wu, K. Naelapää, J.P. Boetker, H. Jensen, J. Rantanen, Simultaneous UV imaging and Raman spectroscopy for the measurement of solvent-mediated phase transformations during dissolution testing, J. Pharm. Sci. 103 (2014) 1149–1156, https://doi.org/10.1002/jps.23883.
[40] F. Ye, A. Yaghmur, H. Jensen, S.W. Larsen, C. Larsen, J. Østergaard, Real-time UV imaging of drug diffusion and release from Pluronic F127 hydrogels, Eur. J. Pharm. Sci. 43 (2011) 236–243, https://doi.org/10.1016/j.ejps.2011.04.015.
[41] A. Ward, K. Walton, K. Box, J. Østergaard, L.J. Gillie, B.R. Conway, K. Asare-Addo, Variable-focus microscopy and UV surface dissolution imaging as complementary techniques in intrinsic dissolution rate determination, Int. J. Pharm. 530 (2017) 139–144, https://doi.org/10.1016/j.ijpharm.2017.07.053.
[42] S. Colombo, M. Brisander, J. Haglöf, P. Sjövall, P. Andersson, J. Østergaard, M. Malmsten, Matrix effects in nilotinib formulations with pH-responsive polymer produced by carbon dioxide-mediated precipitation, Int. J. Pharm. 494 (1) (2015) 205–217.
[43] K. Walton, L. Blunt, L. Fleming, M. Goodhand, H. Lung, Areal parametric

characterisation of ex-service compressor blade leading edges, Wear 321 (2014) 79–86, https://doi.org/10.1016/j.wear.2014.10.007.
[44] K. Walton, L. Blunt, L. Fleming, The topographic development and areal parametric characterization of a stratified surface polished by mass finishing, Surf. Topogr. Metrol. Prop. 3 (2015), https://doi.org/10.1088/2051-672X/3/3/035003.
[45] K. Walton, L. Fleming, M. Goodhand, R. Racasan, W. Zeng, High fidelity replication of surface texture and geometric form of a high aspect ratio aerodynamic test component, Surf. Topogr. Metrol. Prop. 4 (2016), https://doi.org/10.1088/2051-672X/4/2/025003.
[46] Sirius Analytical, Sirius SDi2, 2017. http://www.sirius-analytical.com/products/sdi2 (accessed 09.011.18).
[47] International Standards Organisation, BS EN ISO 25178-2:2012: Geometrical product specifications (GPS). Surface texture. Areal. Terms, definitions and surface texture parameters, 2012 April 30.
[48] X. Pan, T. Julian, L. Augsburger, Quantitative measurement of indomethacin crystallinity in indomethacin-silica gel binary system using differential scanning calorimetry and X-ray powder diffractometry, AAPS PharmSciTech. 7 (2006) E11, https://doi.org/10.1208/pt070111.
[49] M. Colombo, C. Minussi, S. Orthmann, S. Staufenbiel, R. Bodmeier, Preparation of amorphous indomethacin nanoparticles by aqueous wet bead milling and in situ measurement of their increased saturation solubility, Eur. J. Pharm. Biopharm. 125 (2018) 159–168, https://doi.org/10.1016/J.EJPB.2018.01.013.
[50] M. Khanfar, B. Al-Taani, M. Alsmadi, A. Zayed, Enhancement of the dissolution and bioavailability from freeze-dried powder of a hypocholesterolemic drug in the presence of Soluplus, Powder Technol. 329 (2018) 25–32, https://doi.org/10.1016/j.powtec.2018.01.068.
[51] A. Nokhodchi, A. Homayouni, R. Araya, W. Kaialy, W. Obeidat, K. Asare-Addo, Crystal engineering of ibuprofen using starch derivatives in crystallization medium to produce promising ibuprofen with improved pharmaceutical performance, RSC Adv. 5 (2015) 46119–46131, https://doi.org/10.1039/c5ra06183k.
[52] A. Fini, Release problems for nifedipine in the presence of soluplus, J. Pharm. Pharm. 3 (2016) 1–13, https://doi.org/10.15436/2377-1313.16.020.